ATMOSPHERIC AND OCEANIC SCIENCE LETTERS
2020, VOL. 13, NO. 6, 559–567
https://doi.org/10.1080/16742834.2020.1776088

The climate variability in global land precipitation in FGOALS-f3-L: A comparison between GMMIP and historical simulations

TANG Yiqiong[a,b], HE Bian[b,c,d], BAO Qing[b,d], LIU Yimin[b,c,d], LI Jinxiao[b] and WU Guoxiong[b,c,d]

[a]School of Atmospheric Sciences, Nanjing University of Information Science and Technology, Nanjing, China; [b]State Key Laboratory of Numerical Modeling for Atmospheric Sciences and Geophysical Fluid Dynamics (LASG), Institute of Atmospheric Physics, Chinese Academy of Sciences, Beijing, China; [c]CAS Center for Excellence in Tibetan Plateau Earth Sciences, Beijing, China; [d]College of Earth and Planetary Sciences, University of Chinese Academy of Sciences, Beijing, China

ABSTRACT

The climate variability in global land precipitation is important for the global hydrological cycle. Based on the Coupled Model Intercomparison Project Phase 6 (CMIP6) historical experiments and the Global Monsoons Model Intercomparison Project (GMMIP) Tier-1 experiments, the spatial-temporal characteristics of global and regional land precipitation long-term climate changes in CAS FGOALS-f3-L are evaluated in this study. By comparing these two kinds of experiments, the precipitation biases related to the SSTs are also discussed. The results show that the two experiments could capture the precipitation trend and amplitude to a certain degree compared with observations. The GMMIP simulations show a higher skill than the historical runs verified by correlation coefficients partly because the observed monthly mean SST was prescribed. For the Northern Hemisphere, GMMIP can reproduce the trend and variability in global precipitation, while historical simulations cannot reproduce the trend and variability. However, both experiments fail to simulate the amplitude of the southern hemisphere summer precipitation anomalies. Ensemble empirical mode decomposition (EEMD) was applied to compare the simulated precipitation on different time scales. The sea surface temperature anomaly (SSTA) bias, especially the La Niña-type SSTA, is the dominant source of the model bias for simulating interannual precipitation anomalies. The authors also emphasize that the response of precipitation anomalies to the ENSO effect varies regionally. This study highlights the importance of the multiannual variability in SSTAs in global and hemispheric precipitation simulations. The ways to improve the simulation of global precipitation for CAS FGOALS-f3-L are also discussed.

ARTICLE HISTORY
Received 9 March 2020
Revised 21 April 2020
Accepted 26 April 2020

KEYWORDS
CMIP6; GMMIP; global precipitation simulation; climate variability; monsoon simulation

关键词
CMIP6; GMMIP; 全球降水模拟; 气候变率; 季风模拟

FGOALS-f3-L全球陆地降水气候变率评估:GMMIP与historical试验的比较

摘要

全球降水对人们生产生活和经济发展都至关重要。因此，评估模式对降水的模拟能力至关重要。近期大气物理研究所发布了两套CMIP6试验数据，结合GPCC降水资料，本文评估了两组试验对1900–2014年全球陆地降水以及各半球夏季降水模拟性能。结果表明，无论是年际尺度还是长期趋势的模拟，GMMIP试验均表现出更好的模拟性能。考虑到两组试验设计的角度和海温对年际降水的重要影响，本文探讨了全球海温异常尤其是ENSO事件对全球降水和各半球夏季降水的重要性。结果表明，赤道太平洋地区海温对降水模拟影响显著，其影响主要集中在中低纬地区。这对降水模拟的改进有很大帮助。

1. Introduction

Changes in global land precipitation have received much scientific and societal attention due to their impacts on resource administration, ecosystem construction, and economic development. In the past, studies on its climatic change and mechanism encountered obstacles due to the limitation of datasets (Wentz et al. 2007; Adler et al. 2008; Zhou et al. 2008). Numerical simulation can fulfil the vacancy to a certain extent. Prior studies have achieved extensive valuable results using the model simulation and datasets provided by Coupled Model Intercomparison Project Phase 3 (CMIP3) and Coupled Model Intercomparison Project Phase 5 (CMIP5) (Ren et al. 2013). Model projections have indicated on the interannual timescale that the most determinant of variability in global precipitation fields is associated with the El Niño-Southern Oscillation (ENSO) (Smith, Yin, and Gruber 2006; Zhou et al. 2008; Gu and Adler 2013; Gu and Adler 2015). The relationship between global precipitation and Niño3.4 is negative. Global precipitation often decreases in

CONTACT Bian HE heb@lasg.iap.ac.cn

warm event years (Diaz, Bradley, and Eischeid 1989; Dai, Fung, and Del Genio 1997; Curtis and Adler 2003; Gu and Adler 2015). Globally, the first EOF in global precipitation fields is an ENSO-related pattern (Dai, Fung, and Del Genio 1997). Inconsistent responses to the ENSO effect exist in different regions and different seasons (Dai, Fung, and Del Genio 1997; Curtis and Adler 2003). The region with the closest relationship between precipitation and ENSO is the tropics (Diaz, Bradley, and Eischeid 1989). In addition, the signal in the tropics is connected to extratropical precipitation anomalies through meridional atmospheric circulations (Curtis and Adler 2003). On the long-term timescale, increases in global precipitation follow increases in surface temperatures and greenhouse gases (Wentz and Schabel 2000; Wentz et al. 2007; Adler et al. 2008). In addition, the relationship between the SST pattern and global precipitation has been confirmed by simulation and model data diagnosis, which may have implications for the study of rainfall projections (Zhou et al. 2008; Chiang and Friedman 2012; Langenbrunner and Neelin 2013; Gu and Adler 2013, 2015). Except for the ENSO effect, the obvious decrease in global land monsoon precipitation during 1949–2001 was mainly caused by the warming over the central–eastern Pacific and the western tropical Indian Ocean (Zhou et al. 2008; Jiang and Zhou 2019). The remote impact of temperature in the North Atlantic can affect precipitation anomalies through teleconnection (Chiang and Friedman 2012; Gu and Adler 2015).

The precise representation of precipitation has been a consistent focus for the climate community for years because of its scientific significance and great societal and economic implications; it is indeed a common and complex issue in climate models. In attempting to improve climate model simulations, the Coupled Model Intercomparison Project Phase 6 (CMIP6) is designed, and the datasets are currently available (Eyring et al. 2016). The Global Monsoons Model Intercomparison Project (GMMIP) has been endorsed as one of the models intercomparison projects (MIPs) in the CMIP6. The primary goals of GMMIP are to better simulate monsoon climatology and variability and to understand the physical process (Eyring et al. 2016; Zhou et al. 2016). Moreover, the CMIP historical simulations provide rich opportunities to assess model ability to simulate climate, including variability and century timescale trends (Eyring et al. 2016). The external forcing of the two simulations are both prescribed as their monthly mean observation values, as recommended by the CMIP6 projects. In addition, the two simulations define output streams in the centrally coordinated CMIP6 data request so that variables can be stored at the specified frequency and resolution required to address the specific science questions and evaluations (Eyring et al. 2016).

The Chinese Academy of Sciences (CAS) Flexible Global Ocean-Atmosphere-Land System (FGOALS-f3-L) climate system model, which was developed at the State Key Laboratory of Numerical Modeling for Atmospheric Sciences and Geophysical Fluid Dynamics (LASG)/Institute of Atmospheric Physics (IAP) (Zhou et al. 2012, 2015; Bao et al. 2019; He et al. 2019), recently finished GMMIP and historical simulations and released related datasets (He et al. 2019, 2020). It is worth evaluating its performance in precipitation simulations for further model improvement. In this study, our first major objective is to assess the fidelity of precipitation variability in both GMMIP Tier-1 and historical experiments for CAS FGOALS-f3-L. In particular, we intend to evaluate both the interannual variability and long-term trend of precipitation obtained by EEMD here during the 1901–2014 period. From the perspective of SSTA differences, our second major objective is to find the causes of simulation diversity and identify the effect of interannual sea surface temperature on precipitation in CAS FGOALS-f3-L. The outputs from historical and GMMIP Tier-1 simulations can be applied to diagnose the impact from the SSTA bias.

The rest of this paper is organized as follows: Section 2 describes the employed datasets and methods employed for this study. In section 3, the simulated precipitation variability in CAS FGOALS-f3-L is compared with observations, and a possible source of simulation deviation is explored. Finally, a brief summary and a discussion are given in section 4.

2. Data and method

2.1 Datasets

The observational precipitation dataset used in the study is the Full Data Reanalysis provided by the Global Precipitation Climatology Center (GPCC v7). The GPCC dataset for the period 1901–2014 has a spatial resolution of 1°×1°. The GPCC's Full Data product includes monthly precipitation totals of more than 85 000 stations (Schneider et al. 2015). Two sets of simulations, GMMIP Tier-1 and historical experiments, are carried out by CAS FGOALS-f3-L climate system model. The detailed experimental design and model configuration for the two experiments can be found in He et al. (2019, 2020), respectively. Table 1 shows the main differences between the two sets of experiments. The following GMMIP refers to the GMMIP Tier-1 experiment, and 'his' is the abbreviation of historical. The GMMIP outputs last from 1870 to 2014, while the historical runs from 1850 to

Table 1. Brief introduction to the experimental design.

	Experiment_id	Variant_label	Integration time	Experimental design
GMMIP Tier-1	amip-hist	r1i1p1f1	1861–2014	The model integration starts with external forcings defined by the observed datasets, especially sea surface temperature. In addition, the outputs last from 1870 to 2014, and the first nine integration years are recognized as the spin-up time.
GMMIP Tier-1	amip-hist	r2i1p1f1	1862–2014	The same as r1i1p1f1, but the first eight integration years are recognized as the spin-up time.
GMMIP Tier-1	amip-hist	r3i1p1f1	1863–2014	The same as r1i1p1f1, but the first seven integration years are recognized as the spin-up time.
Historical	Historical	r1i1p1f1	1850–2014	The external forcing of sea surface temperature was simulated by the model. In addition, the outputs last from 1850 to 2014.
Historical	Historical	r2i1p1f1	1850–2014	The same as r1i1p1f1.
Historical	Historical	r3i1p1f1	1850–2014	The same as r1i1p1f1.

2014, both with a spatial resolution of 1°×1°. The main difference between the two in experimental design is that the SST was prescribed in GMMIP when simulated in the historical runs. Note that the two simulations contain three experiments, named r1i1p1f1, r2i1p1f1, and r3i1p1f1. Time lag ensemble methods are employed for both experiments.

In addition to precipitation datasets, the Extended Reconstructed Sea Surface Temperature (ERSST) version 3 dataset (Xue, Smith, and Reynolds 2003; Smith et al. 2008) with a spatial resolution of 1°×1° from 1901 to 2014 was applied to explore the rainfall-SSTA relationship. Accordingly, SST obtained from two simulations is also available. The Niño3.4 index was derived from the SST anomaly calculated in the Niño3.4 region (5°S–5°N, 170°W–120°W).

2.2 Method

To understand the simulation of global monsoon precipitation variability of CAS FGOALS-f3-L, we calculated the local summer land precipitation in the northern and southern hemispheres. Local summer is defined from June to August (from December to February) for the Northern (Southern) Hemisphere. When investigating the summer precipitation in the Northern Hemisphere (NH), we evaluated the summer mean (JJA) and regional average of the Northern Hemisphere (0°–90°N) for the seven groups of data, which include the GPCC datasets, three members of the GMMIP and three members of the historical experiment datasets. Similarly, data after a summer mean (DJF) and a regional average of the Southern Hemisphere (0°–90°S) are used to assess the simulation of the Southern Hemisphere (SH). The climatological mean data here are averaged between 1951 and 1980. Additionally, three-member ensemble means of anomalies are computed to reduce internal noise and model uncertainty.

In addition, to evaluate the GMMIP and historical simulation abilities at different timescales exhaustively, we applied the ensemble empirical mode decomposition (EEMD) approach to extract the components from the annual precipitation anomalies. The EEMD is a developed adaptive and temporally local data analysis method based on the empirical mode decomposition (EMD) method (Huang et al. 1998; Huang and Wu 2008), which decomposes a data series into finite components at different frequencies called intrinsic mode functions (IMFs) (Huang et al. 1998; Huang and Wu 2008; Franzke 2010; Franzke and Woollings 2011). In the EMD method, the data series can be decomposed into several IMFs:

$$X(t) = \sum_{i=1}^{n} I_j + r(n), \tag{1}$$

where I_j denotes the j^{th} IMF and $r(n)$ is the residual term after n IMFs are extracted. By adding noise, EEMD eliminates the mode mixing problem to a large extent (Wu and Huang 2009). For more information on the detailed procedure, refer to Wu and Huang (2009). The method has been employed widely to analyse time series and extract trends based on its ability and robustness (Huang and Wu 2008; Wu and Huang 2009; Qian et al. 2009, 2010, 2011; Franzke 2010; Franzke and Woollings 2011). In addition, we can use the counting cross zero numbers method to estimate the averaged period of each component (Qian et al. 2011). We can take each IMF as a wave. The wavelength and wave number can help us estimate the averaged period.

3. Results

3.1 Fidelity of long-term climate variability of land precipitation simulation in FGOALS-f3-L

The observed and simulated annual mean global land precipitation time series from 1850 to 2014 are shown in Figure 1(a). The observed (red line) and ensemble means of the three GMMIP (black lines) and historical (blue lines) simulations are denoted by thick lines. Evident increases and clear interannual and multidecadal variability in annual precipitation are shown in the observations and are well reproduced in both experiments. Separately, GMMIP provides rational amplitude compared with

historical simulations. It is notable that some extreme precipitation years can be captured in the GMMIP simulation. For the boreal summer monsoon precipitation anomaly in the Northern Hemisphere (Figure 1(b)), GMMIP experiments can simulate reasonable precipitation anomalies, such as the one after 1995. Moreover, the two experiments show better simulation of precipitation amplitudes after 1930. For the monsoon simulation in the Southern Hemisphere (Figure 1(c)), it is worth noting that an apparent discrepancy in the precipitation anomaly intensity simulation exists between the simulated and observed results. Specifically, the simulated precipitation anomalies are weaker compared to those observed in both simulations. Obvious positive anomalies can be found in 1917, 1973, and 2010, while negative anomalies can be found in 1965 and 1982. Nevertheless, GMMIP runs still show better simulation performance in detail. For the validation of interannual variation, the correlation coefficients of timeseries between the observations and the two experiments are shown in Table 2. The correlation of precipitation anomalies between the GPCC and GMMIP output ensemble mean is up to 0.700, and r3i1p1f1 is the best. Meanwhile, the correlation between the GPCC and historical runs ensemble mean is 0.404, while r3i1p1f1 shows the best skill of 0.459. The temporal correlation with global annual precipitation is relatively higher than that with hemispheric summer precipitation, presumably resulting from the monsoon precipitation simulation, which involves more complicated physical processes. As depicted in Table 2, the correlation with GMMIP for Northern Hemisphere summer precipitation attains 0.478, while the correlation with historical runs is negative in accordance with Figure 1(b). For south hemispheric summer precipitation, similar to previous results, the correlation with GMMIP reaches 0.358, while the correlation with historical runs reaches 0.086.

Extensive studies have shown that global precipitation variability exhibits different characteristics at

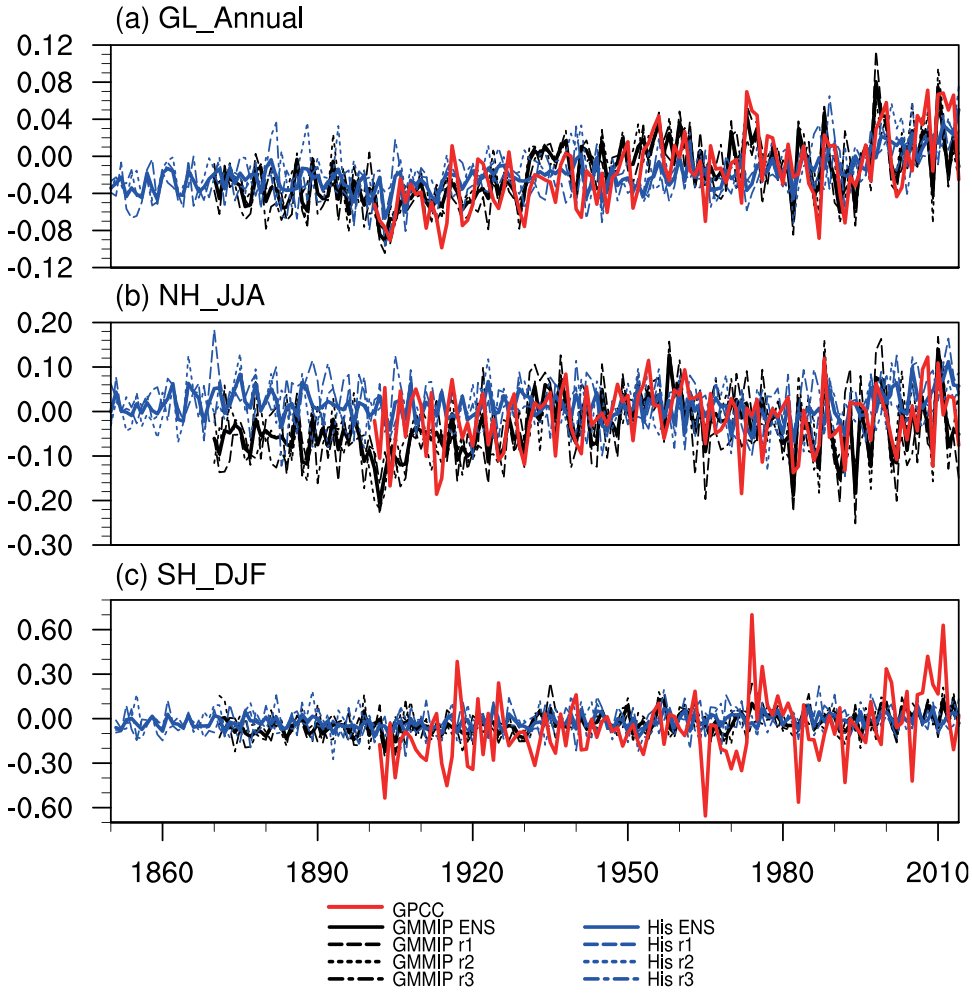

Figure 1. (a) Annual and global averaged land precipitation anomalies (relative to the climatology over 1951–1980). The red, black, and blue solid lines denote GPCC datasets and ensemble mean of GMMIP and historical experiments, respectively. Three kinds of dashed lines represent the three ensemble members: r1i1p1f1, r2i1p1f1, and r3i1p1f1. (b) As in (a) but for summer precipitation in the Northern Hemisphere. (c) As in (a) but for summer precipitation in the Southern Hemisphere (units: mm d^{-1}).

Table 2. Correlation of precipitation anomalies between the two sets of experiments and GPCC. GMMIP refers to GMMIP Tier-1 experiments, and His denotes historical simulations. '*' denotes exceedance of the 95% confidence level, and '**' denotes exceedance of the 99% confidence level.

	ANN(GL)	JJA(NH)	DJF(SH)
GMMIP ENS	0.700**	0.478**	0.358**
GMMIP r1	0.569**	0.330**	0.222*
GMMIP r2	0.653**	0.435**	0.350**
GMMIP r3	0.700**	0.463**	0.276**
His ENS	0.404**	−0.026	0.086
His r1	0.459**	0.186*	0.005
His r2	0.276**	−0.06	0.081
His r3	0.211*	−0.199*	0.068

different timescales, such as ENSO-related interannual variations and AMO-related multidecadal oscillations. (Knight, Folland, and Scaife 2006; Nigam, Guan, and Ruiz-Barradas 2011; Gu and Adler 2015). To investigate the simulation skill of CAS FGOALS-f3-L and to understand the model bias in the simulation of the precipitation climate variability from the perspective of multi-timescale separation, the correlation coefficients between the observations and the three-member ensemble mean of the two experiments are computed after applying EEMD (Table 3). In this study, IMF1 has an average period of approximately 2.8 yr. In addition, the second and third intrinsic mode functions (IMF2, IMF3) correspond to the 5 yr and 16 yr period variability components, respectively; IMF4 denotes the 25 yr period variability component, and the long-term components are composed of trends longer than 40 yr. The ENSO-related pattern with a 5 yr period is most dominant in global precipitation fields (Dai, Fung, and Del Genio 1997), which is also our focus in this study. There is a certain difference between the observed and simulated ENSO-related variability components. Especially for southern hemispheric summer precipitation, the correlations between the observations and the two experiments are negative. However, GMMIP still maintains a better performance compared with historical simulation from the correlation coefficients. It is noteworthy that long-term trends can be reproduced in both experiments, which provides a powerful tool to explore how global precipitation may vary under a warming background, including precipitation magnitude and spatial mode.

In general, the simulation of precipitation climate variability in GMMIP Tier-1 experiments shows better skills than historical runs distinctly at different timescales in both global land precipitation and hemispheric land precipitation. In the next section, SSTAs bias will be taken into account in revealing the possible cause of the simulation difference.

Table 3. Correlation of precipitation anomalies with different timescales between the two experiments and GPCC. GMMIP refers to GMMIP Tier-1 experiments, and His denotes historical simulations. '*' denotes exceedance of the 95% confidence level, and '**' denotes exceedance of the 99% confidence level.

	ANN(GL)	JJA(NH)	DJF(SH)
GMMIP IMF1	0.405**	0.410**	0.121
IMF2	0.303**	0.145	−0.048
IMF3	0.684**	0.110	0.656**
IMF4	0.373**	0.157	0.796**
Long term	0.928**	0.537**	0.874**
His IMF1	−0.214*	−0.143	−0.046
IMF2	0.170	0.052	−0.283**
IMF3	0.314**	−0.187*	0.289**
IMF4	0.189*	0.406**	−0.058
Long term	0.768**	0.261**	0.843**

3.2 Attribution of SSTA bias in the precipitation simulation

In view of the reasonable reproducibility of GMMIP simulation, another question we want to address is the source of simulation discrepancy between two sets of experiments. Previous studies have shown the dominant effect of global SSTs on land surface precipitation changes (Dai, Fung, and Del Genio 1997; Zhou et al. 2008; Gu and Adler 2015). ENSO is a leading component of climate change originating from the tropical Pacific and plays an important role in the spatial structures of global precipitation variability (Gu and Adler 2015). To investigate the impact of SSTA interannual variations on precipitation changes, we next examined the relationship between global precipitation and SSTAs by the regression method. Figure 2 shows a regression map of SSTA onto the IMF2-related GPCC and the simulated ensemble mean of precipitation anomalies. The shadow locates the regions that surpass the 99% confidence level. The green box denotes the Niño3.4 zone. Over the central-eastern equatorial Pacific, the spatial structure of SSTA shows a typical La Niña pattern, which is an essential feature, especially in the annual and JJA mean (Figure 2(a1,b1,a2,b2)). The corresponding strong ENSO pattern extends into the subtropical Pacific and declines substantially in higher latitudes. However, the El Niño-type SSTA pattern is displayed in the historical simulation (Figure 2(c1,c2)). For the DJF mean south hemisphere (Figure 2(a3,b3,c3)), the ENSO signal weakened significantly. At higher latitudes, precipitation anomaly responses in the North Atlantic, though weak, can also be observed. Uniform SSTA signals in the GMMIP simulation agree with observations, while dipole SSTAs exist in historical runs. Consequently, SSTA simulation divergence is one of the sources of the above experimental results difference.

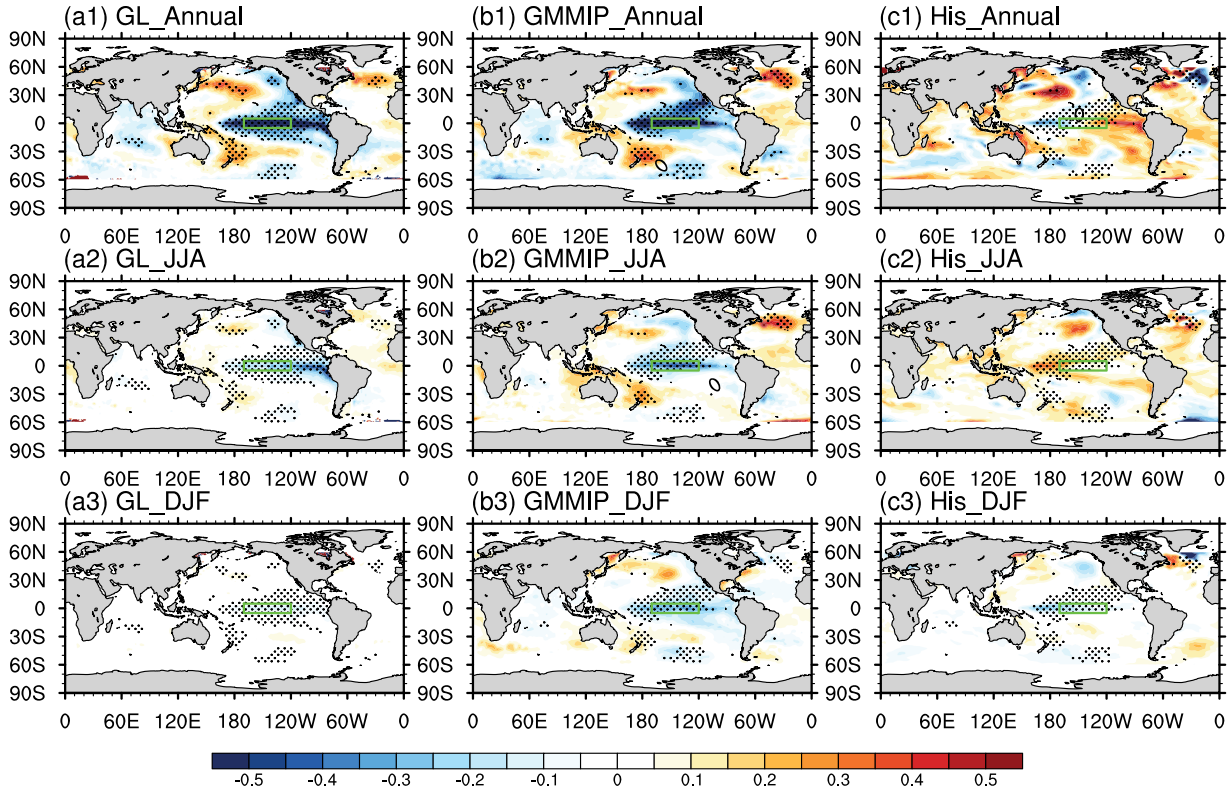

Figure 2. Regression maps of SST anomalies onto IMF2 of precipitation anomalies from (a1–a3) GPCC, (b1–b3) GMMIP, (c1– c3) historical runs over global-and-annual mean (top panel), NH-JJA (middle panel), and SH-DJF (bottom panel). The shadow locates the regions that surpass the 99% confidence level. The green box denotes the Niño3.4 zone.

Regression maps of precipitation anomalies of two simulations against the Niño3.4 index using corresponding SST datasets are constructed to find the areas sensitive to tropical Pacific SST signals owing to the influential ENSO effect. As shown in Figure 3(a1), the ENSO effect on precipitation variability varies from region to region, with a focus on low and mid-latitudes in general, and tends to be weak at higher latitudes. Generally, the observed response is in agreement with Figure 6 in Gu and Adler (2015). For the two experiments (Figure 3(b1,c1)), although relatively large differences can be found in the south-eastern part of Asia, eastern Australia, South America, and central Africa, spatial structures of the observed precipitation anomaly responses to ENSO are well simulated. Beyond doubt, some regions, such as South America, the southern part of North America, and most of Eurasia, are sensitive to the ENSO effect and show spatial patterns that are similar to the observations, but the amplitudes are weaker. Regional pattern differences emerge in the Asian monsoon area, central Africa, and Australia in detail. For Northern Hemisphere summer precipitation, Central Europe, and North America show significantly positive precipitation anomalies, which have been reproduced in two experiments (Figure 3(a2,b2,c2)). Negative precipitation anomalies are displayed in India and eastern China, where the simulations diverge between the two experiments. In addition, details portrayed by the GPCC in East Asia are missed in both experiments. Patterns of the rainfall-SSTA relationship in SH for both experiments are closer to GPCC than in NH except for eastern Australia (Figure 3(a3,b3,c3)). In comparison, it is obvious that the simulation quality of GMMIP runs is better than historical runs from the perspective of the rainfall-SSTA relationship.

Overall, realistic simulation of the SST field is necessary for CAS FGOALS-f3-L to capture the temporal characteristics of global and hemispheric land precipitation.

4. Summary and discussion

In this study, we investigate the primary temporal characteristics of global land precipitation of GMMIP Tier-1 and historical runs from CAS FGOALS-f3-L by comparing with the global monthly precipitation dataset GPCC V7. The CAS FGOALS-f3-L outputs provide considerable information on the global annual precipitation, especially on trend simulations. For the historical and GMMIP Tier-1 experiments, GMMIP shows better performance in reproducing global

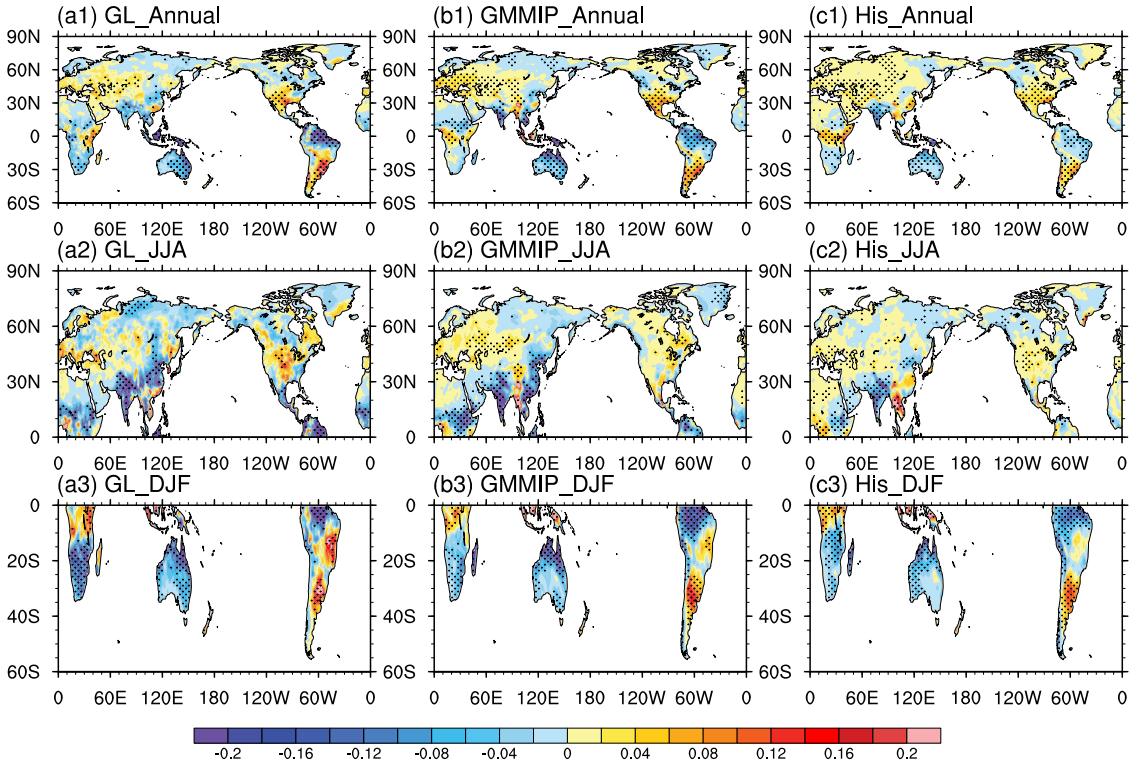

Figure 3. Regression maps of precipitation anomalies from (a1–a3) GPCC, (b1–b3) GMMIP, (c1–c3) historical runs over annual mean (top panel), JJA (middle panel), and DJF (bottom panel) onto the Niño3.4 area-weighted averaged SSTA. The shadow locates the regions that surpass the 95% confidence level.

precipitation variation characteristics in terms of magnitude and trend, with a correlation coefficient up to 0.7. Similarly, GMMIP can reproduce boreal summer precipitation more reasonably with a coefficient up to 0.478, while the correlation between historical simulation and GPCC is negative. Although both experiments fail to simulate the observed magnitude for southern hemispheric summer precipitation, GMMIP simulation shows better capability by comparing the correlation with observations. We use timeseries after EEMD to estimate the climate variability of global precipitation in two sets of experiments.

The attribution of SSTAs bias between the two runs is also explored for model improvement. The rainfall-SSTA relationship manifested in GMMIP outputs is more unanimous with the observations in both magnitude and spatial distribution. The ENSO signal significantly affects global precipitation at low to mid-latitudes, which may lead to performance differences. The North Atlantic SSTA mode effect can also be embodied. The precipitation anomaly response to the ENSO effect varies from region to region. On the interannual timescale, global precipitation anomalies over the Asian-Australian monsoon region are mostly negative, while those in in central Europe and North America are positive. In two experiments, the Asian-Australian monsoon area and central Africa show different patterns from observations, while global precipitation almost tends to be weaker. Hence, corrected SSTA patterns can help us more accurately simulate interannual global land precipitation, especially tropical Pacific SST.

Although the relation between SSTAs and global precipitation has been confirmed by numerous studies, model performance may vary due to differences in model physical processes. Moreover, precipitation simulation is also affected by numerous factors, such as anthropogenic greenhouse gas emissions and surface land temperature, other than SSTAs. Further analysis is necessary to understand the role of model physics and external forcing on reproducing the SSTA-precipitation patterns.

Acknowledgments

We would like to thank the two anonymous reviewers for their suggestions, which have improved the manuscript.

Disclosure statement

No potential conflict of interest was reported by the authors.

Funding

The research presented in this paper was jointly funded by the National Key Research and Development Program of China [Grant No. 2017YFA0604004] and the National Natural Science Foundation of China [Grant Nos. 91737306, 41530426, 91837101, 91937302, and 41606032].

ORCID

Qing BAO http://orcid.org/0000-0003-1719-6540

References

Adler, R. F., G. Gu, J.-J. Wang, G. J. Huffman, S. Curtis, and D. Bolvin. 2008. "Relationships between Global Precipitation and Surface Temperature on Interannual and Longer Timescales (1979–2006)." *Journal of Geophysical Research* 113: D22. doi:10.1029/2008jd010536.

Bao, Q., X. F. Wu, J. X. Li, L. Wang, B. He, X. C. Wang, Y. M. Liu, and G. X. Wu. 2019. "Outlook for El Niño and the Indian Ocean Dipole in autumn-winter 2018–2019." *Chinese Science Bulletin* 64: 73–78. doi:10.1360/N972018-00913.

Chiang, J. C. H., and A. R. Friedman. 2012. "Extratropical Cooling, Interhemispheric Thermal Gradients, and Tropical Climate Change." *Annual Review of Earth & Planetary Sciences* 40 (1): 383–412. doi:10.1146/annurev-earth-042711-105545.

Curtis, S., and R. F. Adler. 2003. "Evolution of El Niño–precipitation Relationships from Satellites and Gauges." *Journal of Geophysical Research* 108 (D4): 4153. doi:10.1029/2002JD002690.

Dai, A. G., I. Y. Fung, and A. D. Del Genio. 1997. "Surface Observed Global Land Precipitation Variations during 1900–88." *Journal of Climate* 10 (11): 2943–2962. doi:10.1175/1520-0442(1997)010<2943:SOGLPV>2.0.CO;2.

Diaz, H. F., R. S. Bradley, and J. K. Eischeid. 1989. "Precipitation Fluctuations over Global Land Areas since the Late 1800's." *Journal of Geophysical Research: Atmospheres* 94 (D1): 1195–1210. doi:10.1029/JD094iD01p01195.

Eyring, V., S. Bony, G. A. Meehl, C. A. Senior, B. Stevens, R. J. Stouffer, and K. E. Taylor. 2016. "Overview of the Coupled Model Intercomparison Project Phase 6 (CMIP6) Experimental Design and Organization." *Geoscientific Model Development* 9 (5): 1937–1958. doi:10.5194/gmd-9-1937-2016.

Franzke, C. 2010. "Long-range Dependence and Climate Noise Characteristics of Antarctic Temperature Data." *Journal of Climate* 23: 6074–6081. doi:10.1175/2010JCLI3654.1.

Franzke, C., and T. Woollings. 2011. "On the Persistence and Predictability Properties of North Atlantic Climate Variability." *Journal of Climate* 24: 466–472. doi:10.1175/2010JCLI3739.1.

Gu, G., and R. F. Adler. 2015. "Spatial Patterns of Global Precipitation Change and Variability during 1901–2010." *Journal of Climate* 28 (11): 4431–4453. doi:10.1175/JCLI-D-14-00201.1.

Gu, G., and R. F. Adler. 2013. "Interdecadal Variability/long-term Changes in Global Precipitation Patterns during the past Three Decades: Global Warming And/or Pacific Decadal Variability?" *Climate Dynamics* 40(11–12): 3009–3022. doi:10.1007/s00382-012-1443-8.

He, B., Q. Bao, X. C. Wang, L. J. Zhou, X. F. Wu, Y. M. Liu, G. X. Wu, et al. 2019. "CAS FGOALS-f3-L Model Datasets for CMIP6 Historical Atmospheric Model Intercomparison Project Simulation." *Advances in Atmospheric Sciences* 36 (8): 771–778. doi:10.1007/s00376-019-9027-8.

He, B., Y. M. Liu, G. X. Wu, Q. Bao, T. J. Zhou, X. F. Wu, L. Wang, et al. 2020. "CAS FGOALS-f3-L Model Datasets for CMIP6 GMMIP Tier-1 and Tier-3 Experiments." *Advances in Atmospheric Sciences* 37 (1): 18–28. doi:10.1007/s00376-019-9085-y.

Huang, N. E., Z. Shen, S. R. Long, M. C. Wu, H. H. Shih, Q. Zheng, N. C. Yen, C. C. Tung, and H. H. Liu. 1998. "The Empirical Mode Decomposition and the Hilbert Spectrum for Nonlinear and Non-stationary Time Series Analysis." *Proceedings A* 454 (1971): 903–995. doi:10.1098/rspa.1998.0193.

Huang, N. E., and Z. H. Wu. 2008. "A Review on Hilbert-huang Transform: Method and Its Applications to Geophysical Studies." *Reviews of Geophysics* 46: RG2006. doi:10.1029/2007RG000228.

Jiang, J., and T. Zhou. 2019. "Global Monsoon Responses to Decadal Sea Surface Temperature Variations during the Twentieth Century: Evidence from AGCM Simulations." *Journal of Climate* 32 (22): 7675–7695. doi:10.1175/JCLI-D-18-0890.1.

Knight, J. R., C. K. Folland, and A. A. Scaife. 2006. "Climate Impacts of the Atlantic Multidecadal Oscillation." *Geophysical Research Letters* 33: L17706. doi:10.1029/2006GL026242.

Langenbrunner, B., and J. D. Neelin. 2013. "Analyzing ENSO Teleconnections in CMIP Models as a Measure of Model Fidelity in Simulating Precipitation." *Journal of Climate* 26 (13): 4431–4446. doi:10.1175/JCLI-D-12-00542.1.

Nigam, S., B. Guan, and A. Ruiz-Barradas. 2011. "Key Role of the Atlantic Multidecadal Oscillation in 20th Century Drought and Wet Periods over the Great Plains." *Geophysical Research Letters* 38: L16713. doi:10.1029/2011GL048650.

Qian, C., C. Fu, Z. Wu, and Z. Yan. 2009. "On the Secular Change of Spring Onset at Stockholm." *Geophysical Research Letters* 36: L12706. doi:10.1029/2009GL038617.

Qian, C., Z. Wu, C. Fu, and D. Wang. 2011. "On Changing El Niño: A View from Time-varying Annual Cycle, Interannual Variability and Mean State." *Journal of Climate* 24 (24): 6486–6500. doi:10.1175/jcli-d-10-05012.1.

Qian, C., Z. Wu, C. Fu, and T. Zhou. 2010. "On Multi-timescale Variability of Temperature in China in Modulated Annual Cycle Reference Frame." *Advances in Atmospheric Sciences* 27: 1169–1182. doi:10.1007/s00376-009-9121-4.

Ren, L., P. Arkin, T. M. Smith, and S. S. P. Shen. 2013. "Global Precipitation Trends in 1900-2005 from a Reconstruction and Coupled Model Simulations." *Journal of Geophysical Research: Atmospheres* 118 (4): 1679–1689. doi:10.1002/jgrd.50212.

Schneider, U., A. Becker, P. Finger, A. Meyer-Christoffer, B. Rudolf, and M. Ziese. 2015. "GPCC Full Data Monthly Product Version 7.0 At 1.0°: Monthly Land-Surface Precipitation from Rain-Gauges Built on GTS-based and Historic Data." doi:10.5676/DWD_GPCC/FD_M_V7_100.

Smith, T. M., R. W. Reynolds, T. C. Peterson, and J. Lawrimore. 2008. "Improvements to NOAA's Historical Merged Land–ocean Surface Temperature Analysis (1880–2006)." *Journal of Climate* 21: 2283–2296. doi:10.1175/2007JCLI2100.1.

Smith, T. M., X. Yin, and A. Gruber. 2006. "Variations in Annual Global Precipitation (1979–2004), Based on the Global Precipitation Climatology Project 2.5° Analysis." *Geophysical Research Letters* 33: L06705. doi:10.1029/2005GL025393.

Wentz, F. J., L. Ricciardulli, K. Hilburn, and C. Mears. 2007. "How Much More Rain Will Global Warming Bring?" *Science* 317 (5835): 233–235. doi:10.1126/science.1140746.

Wentz, F. J., and M. Schabel. 2000. "Precise Climate Monitoring Using Complementary Satellite Data Sets." *Nature* 403 (6768): 414–416. doi:10.1038/35000184.

Wu, Z. H., and N. E. Huang. 2009. "Ensemble Empirical Mode Decomposition: A Noise-assisted Data Analysis Method." *Advances in Adaptive Data Analysis* 01 (1): 1–41. doi:10.1142/S1793536909000047.

Xue, Y., T. M. Smith, and R. W. Reynolds. 2003. "Interdecadal Changes of 30-yr SST Normals during 1871–2000." *"Journal of Climate* 16: 1601–1612. doi:10.1175/1520-0442-16.10.1601.

Zhou, L. J., Q. Bao, Y. M. Liu, G. X. Wu, W. C. Wang, X. C. Wang, B. He, H. Y. Yu, and J. D. Li. 2015. "Global Energy and Water Balance: Characteristics from Finite-volume Atmospheric Model of the IAP/LASG (FAMIL1)." *Journal of Advances in Modeling Earth Systems* 7 (1): 1–20. doi:10.1002/2014MS000349.

Zhou, L. J., Y. M. Liu, Q. Bao, H. Y. Yu, and G. X. Wu. 2012. "Computational Performance of the High-Resolution Atmospheric Model FAMIL." *Atmospheric and Oceanic Science Letters* 5 (5): 355–359. doi:10.1080/16742834.2012.11447024.

Zhou, T. J., A. G. Turner, J. L. Kinter, B. Wang, Y. Qian, X. L. Chen, B. Wu, et al. 2016. "GMMIP (V1.0) Contribution to CMIP6: Global Monsoons Model Inter-comparison Project." *Geoscientific Model Development* 9 (10): 3589–3604. doi:10.5194/gmd-9-3589-2016.

Zhou, T. J., R. Yu, H. Li, and B. Wang. 2008. "Ocean Forcing to Changes in Global Monsoon Precipitation over the Recent Half-century." *Journal of Climate* 21 (15): 3833–3852. doi:10.1175/2008JCLI2067.1.